5 Conclusions

5.1 Summary of the MSSTA III data

The MSSTA III obtained 84 spectroheliograms in 5 EUV (150 Å, 171 Å, 180 Å, 195 Å, 211 Å) and 2 FUV (1216 Å and 1550 Å) bandpasses. Several of these bands that are well-studied, but some (the 150 Å and 211 Å) have never before been imaged at high resolution. Four of the MSSTA telescopes failed to record images; in three of the four cases, this was due to the failure of their Zirconium visible-light rejection filters under the concentrated solar flux. These failures limited our ability to study upper transition region plasma. The resolution of the EUV images is limited to about 10 arc-seconds by the graininess of the film used to record their images. Furthermore, the 150 Å and 180 Å telescopes were slightly misaligned, and thus include just over half the area of the solar disk in their images. The FUV images are full-disk, and are noticeably sharper than the EUV.

Extensive work was done to ensure accurate photometric calibration of the MSSTA telescopes. Prior to flight, we estimated the calibration accuracy at 25-35%, with the largest component of the error coming from the film response curve. Unfortunately, there are indications that the calibration of the EUV images is off by up to a factor of 8. While the overall statistical noise in the MSSTA measurements is of roughly the expected size, the large systematic errors are extremely troubling, particularly in light of our findings regarding the sensitivity of DEM extraction to error. The images were renormalized to bring them into agreement with the photometric calibration of EIT by adjusting the film calibration after flight.

Nevertheless, the MSSTA images constitute a unique and powerful dataset. In combination with observations from EIT and TRACE, they can be used to probe the thermal structure of the solar atmosphere in the range 300,000 K < T < 3,000,000 with unprecedented breadth and accuracy.

They offer a badly-needed remedy to the problem of underconstraint that has plagued past quantitative analyses based on multilayer images.

5.2 Summary of the DEM reconstruction results

Any dataset consisting of measurements of EUV line intensities (or, in the case of narrowband imagers, some combination of EUV line intensities) can be used to place constraints on the differential emission measure of the emitting plasma. By making some simplifying assumptions, we can see that the DEM contains all the information about the configuration and conditions of the observed material that can possibly be derived from such observations. Therefore, extracting DEMs from multilayer observations, and understanding the precision of those DEMs is an essential step in realizing the diagnostic power of multilayer telescopes.

I explored the problem of characterizing the thermodynamic state of an emitting plasma based on narrowband observations, and found that conventional techniques like the filter-ratio method and two-bandpass forward modeling do not generally lead to reliable and unique solutions. However, a suite of simultaneous, co-aligned images in at least five distinct bandpasses can be used to extract full and accurate DEMs. Treating the extraction as an inverse problem leads to the conclusion that the transformation is ill-conditioned due to the broad temperature response of the line contribution functions. Therefore, the inversion is extremely sensitive to noise and error.

Taking a forward approach to the problem allows us to test the performance of the DEM extraction with simulated data. We find that, while additional bandpasses are useful in extending the applicable range of the recovered DEM, the amount of error in the dataset is absolutely critical to the success of the DEM extraction. At 10%, the DEM can be obtained quite reliably; at 25%, the recovery has some value but is suspect, and errors much larger than that render the recovery process almost completely untrustworthy. The precise nature of the error must be understood: while random errors were most thoroughly studied, systematic errors can be much more damaging. Systematic errors that effect all bands equally, on the other hand, lead to an overall normalization error in the best-fit DEM, but do not distort its shape.

Using the re-normalized MSSTA images and EIT images taken shortly before, I was able to find DEM functions describing the full solar disk, a characteristic active region and a quiet region, and smaller-scale DEMs describing 30 arc-second square subregions on the disk. The recovered DEMs generally reproduced more than half the observations to within 25%, and virtually all to within 50%. The most noteworthy, persistent feature of the recovered DEMs was a dip at 10^6 K, suggesting that most of the emission seen in the MSSTA images comes from either cooler or hotter plasma. This finding is not in agreement with the prevailing view of the temperature structure of the solar atmosphere.

It may be possible to account for this result with theoretical arguments based on reconsidering the amount of conductive heating between the corona and the chromosphere. However, it is more likely an indication of the inability of the selected multilayer observations to provide firm constraints on the shape of the coronal DEM. In light of this difficulty, further quantitative analysis of those observations (or similar ones) must be considered highly suspect.

5.3 Future Prospects

From the beginning, the MSSTA project has been a two-pronged effort to extract precise quantitative information about the state of the corona by obtaining a novel data set and applying innovative analysis techniques. The primary result of this work has been, not a new understanding of the physics of the sun, but a deeper awareness of the limitations of existing datasets and of the challenges involved in constraining models of the corona. While a certain amount of disappointment is inevitable, that does not mean that this result is not useful or interesting; its implications for our understanding of coronal structures are potentially quite broad. Many of the conclusions presented in the solar literature of the last several years must be re-examined based on a full appreciation of the extent and effect of uncertainty in multilayer images.

Furthermore, the data obtained by the MSSTA III and the procedures developed after its flight have not exhausted their utility yet. The fact that the data are insufficient to constrain a DEM implies that the types of analyses performed on past MSSTA data sets, such as physical modeling of x-ray bright points or funnels, are inappropriate, but the data set is varied and flexible enough that it could be used in a number of other ways. In addition, the DEM extraction procedure may prove extremely valuable when combined with the observations of instruments now in their planning stages. In this section, I will briefly discuss some future applications that might make use of the MSSTA results.

5.3.1 APPLICATIONS OF MSSTA III DATA

The best way to improve the analysis of any given set of data is to incorporate more data. The stability of the quantitative analysis of the MSSTA EUV images could be improved by using other data sets to add more constraints to the recovered DEM. There are no candidates for inclusion in such an analysis that would not require some sacrifices; the three EUV channels on EIT are the only observations that can be easily combined with the MSSTA images without loss of spatial coverage, resolution or ease of execution.

However, vast amounts of solar data taken around the time of the MSSTA III launch could be used with some care. Full-disk calibrated spectra from TIMED-SEE have already been brought in to re-calibrate the MSSTA images, but these spectra can be used to derive a full-disk DEM which would constitute a valuable additional constraint on the spatially-resolved DEMs obtained by the MSSTA. CDS and SUMER observations could similarly provide reference DEMs for subsets of the MSSTA field of view. Though it is not optically thin, EIT's 304 Å bandpass could give an approximate constraint on the low-temperature end of the DEM curve, and help eliminate the suspiciously large peak of cool material suggested by some of the MSSTA results.

The MSSTA III data could of course be studied in the way that data from its predecessors was generally used: to constrain physical models of coronal structures. The problems of uniqueness and noise sensitivity that arise from using multilayer images in this manner could be somewhat alleviated by incorporating magnetograms or FUV or visible-wavelength observations in the same forward models.

The FUV data of the MSSTA III have not been used at all, which seems wasteful considering their excellent spatial resolution (especially for the 1550 Å telescope) and spectral purity (especially for the 1216 Å telescope). These images could certainly prove valuable for forward modeling of physical structures; in particular, Lyman α emission has been used as a proxy for conductive flux at the base of the transition region (Kankelborg, Walker et al. 1996). More recent observations have suggested that back-conduction is insufficient to account for the bulk of the disk Lyman α emission (Vourlidas, Klimchuk et al. 2001), but even if only a handful of bright footpoint-type structures seen in the MSSTA 1216 Å image can be fit by tweaking the coronal loop models of (Aschwanden, Schrijver et al. 2001) and applying them to the corresponding structures seen in the MSSTA EUV images, the implications for the debate on the interconnectivity of the various layers of the solar atmosphere would be significant.

An intriguing possible application of the MSSTA data was suggested during the attempt to correct the images for the effects of atmospheric absorption (see Section 3.3.1). Existing atmospheric models like the MSIS model have uncertainties of 20-50% in the parameters that determine the EUV absorption cross-section as a function of altitude. The MSSTA provides a

wonderfully uncomplicated set of soundings of the EUV absorption characteristics of the Earth's atmosphere in the range of 150 – 270 km, if we treat the sun as a back-light of roughly constant intensity (which it is, over the duration of the flight, at sufficiently large spatial scales). While the calibration uncertainties in the MSSTA data may render them useless for this application, only relative calibration accuracy is necessary; and state-of-the-art atmospheric models are based on analysis of substantially less applicable data (Zhitnik, Boyarchuk et al. 2003).

5.3.2 APPLICATIONS OF THE DEM RECONSTRUCTION TECHNIQUE

The success of the last generation of multilayer instruments, from the MSSTA I and II through EIT and TRACE to the MSSTA III, has made high-resolution EUV images an increasingly essential part of our understanding of the corona. As a result, most large-scale solar missions planned for the coming decade rely to some extent, directly or indirectly, on multilayer imagers. Improvements in detectors, deposition processes and spacecraft systems will pave the way for increasingly powerful versions of these highly successful instruments.

The next generation of narrowband multilayer telescopes is typified by the Atmospheric Imaging Assembly on the Solar Dynamics Observatory, scheduled for launch in 2008. The AIA design combines the advantages of TRACE (high cadence and spatial resolution) and EIT (continuous, long-term full-disk coverage) with an essentially MSSTA-like approach to multilayer imaging, emphasizing the importance of simultaneous, full-disk images in six EUV bandpasses using an array of telescopes. Its dataset is expected to have the following properties:

- It will consist of images in EUV bandpasses centered on strong iron emission lines at 94 Å, 133 Å, 171 Å, 195 Å, 211 Å, and 335 Å;
- White-light and FUV images at the same scale will be obtained concurrently;
- Each EUV channel will record continuous image sequences with a cadence of ~ 10-15 seconds (using four telescopes, with two channels on each telescope, and alternating between the channels);
- Each image will be 16 Megapixels, covering the full solar disk with ~1 arc-second pixel-limited spatial resolution;

- Near-continuous coverage throughout the mission is possible thanks to the inclined geosynchronous orbit of the SDO (which does result in eclipse seasons twice per year).

The AIA represents the best chance yet at grasping the holy grail described in Chapter 1: DEM functions obtained for lines of sight all over the solar disk with high cadence and high spatial resolution. Indeed, DEM extraction is one of the primary science goals of the AIA, and simulated AIA data have already been used to test a variety of DEM-recovery algorithms similar to those presented in Chapter 4 (Weber, DeLuca et al. 2004). (A related group is pursuing a more sophisticated, but much less efficient, Markov-Chain Monte-Carlo approach to DEM reconstruction (Lin, Kashyap et al. 2004) that can incorporate broad-band imagers; they are testing their algorithm against simulated data from the planned Solar-B mission.)

Discussions and code-exchanges with Weber *et al.* have confirmed that their forward-fitting algorithm is essentially identical to the one I used on the MSSTA images. How, then, to explain their finding that AIA observations will be sufficient to constrain DEMs over the range Log(T) = 5.5 – 7.5 with a temperature resolution of ~ 0.2 in Log(T) and an accuracy of ~ 5%? The results of Chapter 4 suggest that MSSTA and EIT, with a similar number of bandpasses, cannot constrain the DEM at three temperatures from 5.8 – 6.4 to better than ~ 50%. Certainly the AIA channels are well-chosen, providing broader temperature coverage and less overlap than the combined MSSTA and EIT dataset. However, most of the discrepancy is due to different treatment of error and uncertainty in the two sets of simulations. Weber *et al.* simulate ~ 3% uncorrelated statistical error on each bandpass; their simulations do not explicitly consider the effect of systematic errors, although they estimate (based on a separate analysis) that systematic errors in a single channel are tolerable up to ~ 15%.

While it is true that the approximation I have made in treating systematic errors as random errors uncorrelated between the various bandpasses is a crude one, it cannot be denied that systematic errors are present and will continue to be present in all the EUV bandpasses of even an extremely well-calibrated instrument at levels greater than 20%. Moreover, the correlations that exist between these systematic errors cannot be reliably assumed to be perfect, so there is no justification for assuming that these uncertainties will result in an overall normalization error rather than a distortion in the shape of the recovered DEM. Indeed, the distortion of the DEM

result is amplified in proportion to the temperature resolution used by the recovery algorithm, so the more ambitious a DEM-extraction routine becomes, the more sensitive it becomes to systematic errors. The implications of these considerations, and a more subtle approach to modeling the effect of uncertainty on AIA data, are under discussion with Weber *et al.*

The AIA is certainly not the last word on coronal DEM-measuring instruments; payloads with still more bandpasses, telescopes with still better spatial, temporal and spectral resolution, instruments and databases with ever more reliable calibration can be designed and built. As we work towards such instruments, the lessons learned in the analysis of the MSSTA data will be worth revisiting once more. A careful selection of EUV bandpasses based on the narrowness and separation of the individual channels' temperature responses (expressed quantitatively through the SVD of the kernel matrix) should be the starting point of any instrument design. Algorithms that balance accuracy with suppression of noise should be developed and tested on simulated data before the instrument is built. And finally, an understanding of the nature and effect of uncertainty on the analysis of the results is absolutely critical if multilayers are to be used to improve our still-vague quantitative understanding of the corona.

EUV multilayers are powerful tools that have already revolutionized solar physics, and have the potential to provide final answers to some of the most puzzling problems in the field. But the fact is that the current generation of multilayer instruments is limited by large uncertainties in instrument calibration and knowledge of atomic processes. Even if these practical challenges can be overcome, future multilayer imagers will still face fundamental limitations due to the line-of-sight confusion inherent in observations of an optically thin plasma, and to the broad temperature range over which EUV emission lines are radiated. Multilayers are not magic mirrors; they do not tell us the whole story; they do not render other types of instruments, and physical intuition, obsolete; and, no matter how advanced the telescopes and the analysis routines become, they never will.

5.4 The ATSSI

It is unlikely that the MSSTA experiment will be flown again. At best, if the instrument could be reconfigured with new filters and multilayers and upgraded with CCD detectors as described in the previous chapter, it might return a dataset with more images, superior resolution, and better coverage of the upper transition region than we achieved with the MSSTA III. However, the generation of solar observatories scheduled for launch in the next three years (including Solar-B, STEREO, and especially the AIA instrument on SDO) will return enough high-quality data to render even an improved MSSTA IV obsolete.

Nevertheless, sounding rockets can still play an important role in the development of our understanding of the corona. In particular, they offer a relatively low-cost, high-speed platform for assessing the viability of novel observational techniques. In this chapter, I describe a proposed design for the Advanced Technology Solar Spectroscopic Imager (ATSSI) – a sounding rocket experiment using the MSSTA truss that will test the suitability of several promising new technologies for coronal observations. The chapter is adapted from (Boerner, Martínez-Galarce et al. 2004), which was presented at the LTD-10 conference in Genoa, Italy in July 2003.

5.4.1 ABSTRACT

The Advanced Technology Solar Spectroscopic Imager (ATSSI) is a sounding rocket-borne experiment that will employ a Transition-Edge Sensor (TES) placed at the focus of a Wolter-I mirror to study large active region loops in the solar corona. The TES instrument will operate in the ~ 500 – 1500 eV EUV/soft X-ray bandpass, obtaining ~ 3 eV energy-resolved spectra at ~ 6.25 arc-second image resolution with a count rate of ~ 1000 photons/sec/pixel. Over a typical observation period of ~360 sec, we will raster scan over a 0.6 x 0.6 arc minute field of view to obtain a 6 x 6 pixel image containing true EUV/soft X-ray spectroheliograms of a solar active region. Using these observations, we can directly determine composition, electron density and thermal differential emission measure of large active region loops in order to constrain models of

heating mechanisms and accurately measure the thermal morphology of these structures. In the current analysis, we present an initial instrument concept and discuss some of the mission science goals.

5.4.2 INTRODUCTION

The Advanced Technology Solar Spectroscopic Imager (ATSSI) (Wamba, Walker et al. 2000) is a sounding-rocket borne observatory that will debut the use of a Transition-Edge Sensor (TES) and replicated grazing-incidence optic to measure the solar corona in the 500–1500 eV EUV/soft X-ray spectral range with ~3 eV resolution.

Obtaining high-energy spectral observations in conjunction with high spatial resolution imaging is imperative to understanding the temporal, spatial and thermal morphology of the solar atmosphere. Armed with highly resolved spectra at every imaged point, we will be able to further constrain models of coronal structures (e.g. small and large loops, funnels, bright points, spicules, etc.). Such highly detailed information regarding dynamics, magnetic morphology and elemental abundance will give us further clues toward understanding the complex nature of the sun. In the present analysis we briefly discuss the ATSSI instrument and present a representative active region solar spectrum we could expect to observe using a TES.

5.4.3 ATSSI SYSTEM CONCEPT

The ATSSI will be built on the truss structure of the Multi-Spectral Solar Telescope Array (MSSTA) rocket payload, which has successfully flown three times. ATSSI will fly a single TES pixel at the focus of a Wolter I mirror. The TES instrument will be pointed at an active region on the sun, and, using the rocket's Attitude Control System, we will raster scan a 6 x 6 pixel image array. The dwell time of ~10 seconds at each 6.25 arc-second pixel should be short enough to avoid distortion in the image caused by motion of small-scale coronal sources. (This deviates from the original concept of flying an 8x8 array that has proven more complex and costly.(Boerner, Martínez-Galarce et al. 2004))

The primary technical challenge of the mission will be to maintain the TES detector at its operating temperature of ~80 mK throughout the mission (particularly during launch). The cryostat will be an adiabatic demagnetization refrigerator (ADR), based on the one that was launched three times by McCammon et al. beginning in 1996 (McCammon, Almy et al. 2002). This system will be modified by introducing a combination of active and passive magnetic shielding in order to isolate the TES and SQUID amplifiers from the cryostat's strong magnetic field.

The detector itself will be a superconducting bilayer TES developed at NIST (Wollman, Nam et al. 2000). The detectors are fabricated as Mo/Cu bilayers on a Si_3N_4 membrane with a base Si substrate. Because of the steepness of the superconducting transition, the measurement of the photon energy is very accurate ($\Delta \lambda \sim 3$ eV at 1.5 keV for ATSSI), resulting in a highly efficient, high resolution detector. Although better energy resolution has been achieved (~2.0 eV (Wollman, Nam et al. 2000)), we expect to suffer some degradation in resolution from pileup caused by the high solar flux.

In the present design, the Wolter telescope that feeds the detector will have an aperture of 125 mm and a focal length of 1820 mm. The geometrical collecting area of the optic is approximately 7 cm^2. The mandrels for the paraboloidal and hyperboloidal mirror sections will be precision diamond turned and flow-polished to the desired shape, and inspected for roughness and figure errors using optical interferometry and atomic force microscopy. The mirrors will then be constructed using a replication technique against the mandrels. Precisely controlled build-up of a ruthenium shell results in a finished internal paraboloid and hyperboloid, each 100mm long, with a grazing angle of 1° on each segment. Because the ATSSI uses a single-pixel detector, off-axis aberrations are not a significant concern.

It is important to keep out-of-band photons from reaching the detector, and to make sure that the count rate of in-band photons does not saturate the detector. The size and efficiency of the Wolter mirror are such that the unfiltered x-ray flux is several orders of magnitude higher than the detector is capable of counting. However, we have flexibility in filtering the flux and can use an assortment of different filter materials so that their absorption edges define a narrow energy

window. The proposed filter stack uses a series of 5 filters, each consisting of a 4000 Å polyimide film with a 1500 Å aluminum coating on one side. The first filter will be placed at the telescope's entrance aperture to reject most of the visible and infrared light before it reaches the Wolter mirror shell, ensuring that the optic will not heat up and deform and that the filter will not be damaged by the concentrated solar flux. The rest of the filter stack will be placed between the optic and the detector. Those closest to the detector will need to be cooled in stages (130, 30 and 2K) in order to reduce infrared emission from the filters themselves. (In a separate analysis, we intend to more precisely determine the cooled filter stack and the impinging thermal load and infrared photon count rate.) The filters will be fabricated by Luxel Corp., who has built filters for the MSSTA missions, as well as TRACE and other extreme ultraviolet/soft x-ray observatories.

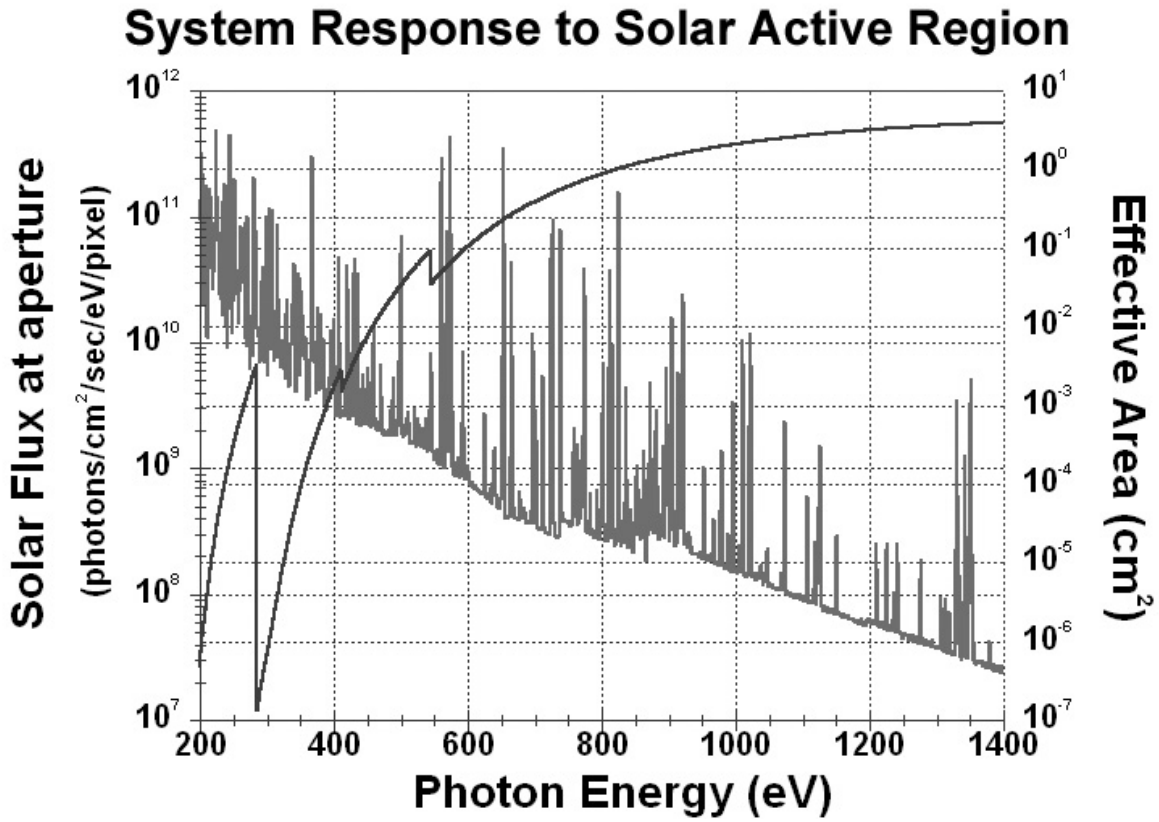

Figure 76. Effective area (collecting area times efficiency) of the ATSSI telescope and filters, superimposed on a simulated spectrum from a solar active region at the aperture of the ATSSI.

Figure 76 shows the effective area of the ATSSI instrument. Its response is dominated by the transmission of the filter stack, which strongly attenuates flux from EUV lines and continuum below 400 eV, as well as rejecting visible and infrared light. The mirror material and grazing

angle were chosen so that throughput from the optic is essentially constant over the energy range of interest (500-1500 eV). The mirror reflectivity begins to drop very sharply at about 2500 eV, and defines the upper end of the ATSSI's energy window (solar active regions, however, do not emit strong lines beyond 1500 eV).

5.4.4 AN ACTIVE REGION IN THE X-RAY

Superimposed on the throughput in Figure 1 is the expected emission over the energy range of the ATSSI bandpass from a solar active region. It was calculated using the CHIANTI database (Dere, Landi et al. 1997). The spectrum contains a continuum component that is strongest at low energies; at higher energies, it is characterized by strong, well-isolated emission lines from highly ionized iron, oxygen and other elements.

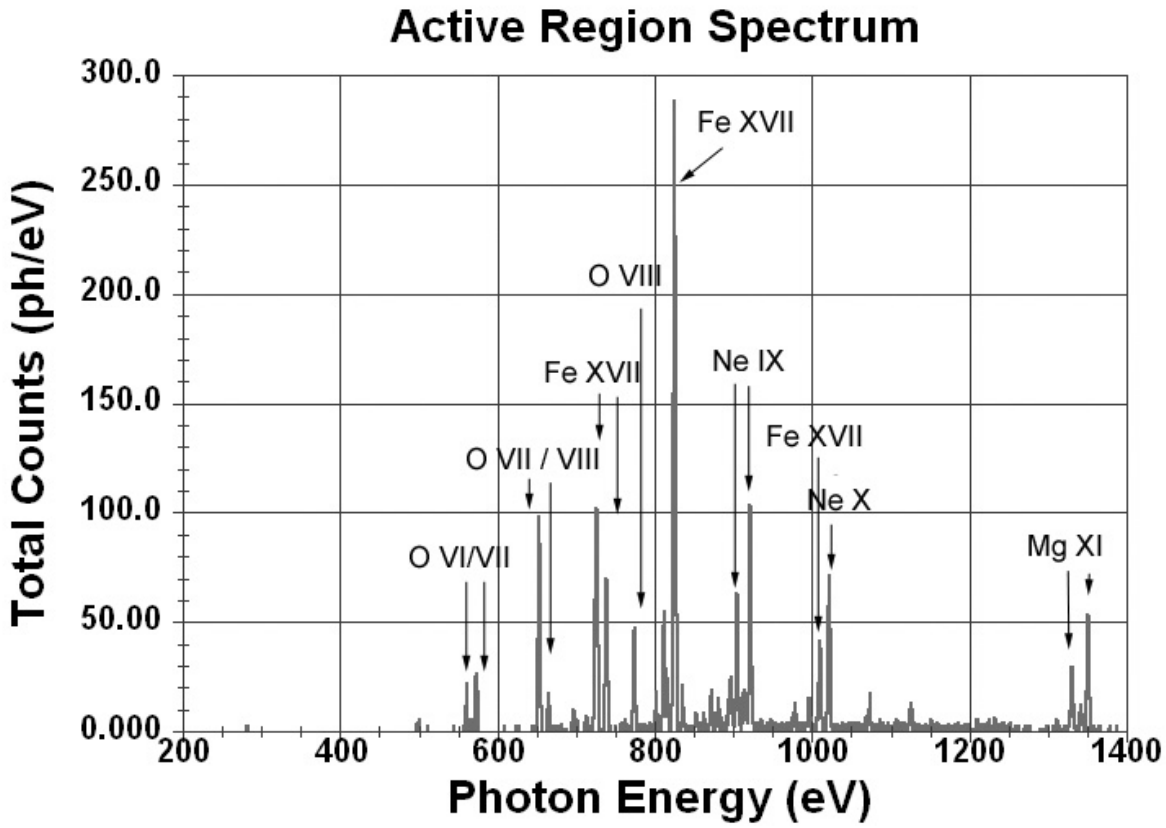

Figure 77. Simulated result of a 10-sec, single pixel (~6.25 arcsec), observation of an active region by ATSSI.

Figure 77 contains the results of a simulation of what the ATSSI data might look like given the solar spectrum and instrument response of Figure 76. Because the TES counts individual photons, the number of photons from a particular emission line which reach the detector was chosen based on Poisson statistics. The effect of the instrument's 3 eV resolution was simulated by assigning each photon to an energy bin chosen from a Gaussian distribution with FWHM of 3 eV. The continuum was also included in the simulation; however, few continuum photons contribute to the final spectrum.

A total of 16 emission lines are detected at a signal-to-noise ratio of at least 10:1. The energy resolution of the detector is not sufficient to detect Doppler shifts from any but the fastest plasma flows (~few hundred km/s). However, simply measuring fluxes in these lines provides a wealth of diagnostic information about the condition of the coronal plasma. The contribution functions for

the lines in the ATSSI bandpass span the temperature range $T = 10^6 – 10^7$, thereby constraining the thermal differential emission measure over that range. This knowledge of the temperature and density distribution of material can be used to generate models of the structures responsible for this emission and to test theoretical coronal heating functions. Temperature-sensitive line ratios of O VII and Fe XVII can be measured as a further diagnostic tool. This observational technique will yield a wealth of important clues about the corona.